frontiers | Frontiers in Energy Research

TYPE Original Research
PUBLISHED 29 December 2023
DOI 10.3389/fenrg.2023.1305492

OPEN ACCESS

EDITED BY
Jianli Zhou,
Xinjiang University, China

REVIEWED BY
Mohamed Salem,
University of Science Malaysia (USM), Malaysia
Kun Wang,
Hebei University of Technology, China
Cheng Xu,
North China Electric Power University, China

*CORRESPONDENCE
Zhang Bai,
baizhang@upc.edu.cn

RECEIVED 01 October 2023
ACCEPTED 11 December 2023
PUBLISHED 29 December 2023

CITATION
Su W, Li Q, Wang S, Zheng W, Bai Z, Han Y and Yu Z (2023), Operating characteristics analysis and capacity configuration optimization of wind-solar-hydrogen hybrid multi-energy complementary system.
Front. Energy Res. 11:1305492.
doi: 10.3389/fenrg.2023.1305492

Operating characteristics analysis and capacity configuration optimization of wind-solar-hydrogen hybrid multi-energy complementary system

Wei Su[1], Qi Li[2], Shuoshuo Wang[2], Wenjin Zheng[1], Zhang Bai[2]*, Yunyi Han[2] and Zhenyue Yu[1]

[1]Powerchina HuaDong Engineering Corporation Limited, Hangzhou, China, [2]College of New Energy, China University of Petroleum (East China), Qingdao, China

Wind and solar energy are the important renewable energy sources, while their inherent natures of random and intermittent also exert negative effect on the electrical grid connection. As one of multiple energy complementary route by adopting the electrolysis technology, the wind-solar-hydrogen hybrid system contributes to improving green power utilization and reducing its fluctuation. Therefore, the moving average method and the hybrid energy storage module are proposed, which can smooth the wind-solar power generation and enhance the system energy management. Moreover, the optimization of system capacity configuration and the sensitive analysis are implemented by the MATLAB program platform. The results indicate that the 10-min grid-connected volatility is reduced by 38.7% based on the smoothing strategy, and the internal investment return rate can reach 13.67% when the electricity price is 0.04 $/kWh. In addition, the annual coordinated power and cycle proportion of the hybrid energy storage module are 80.5% and 90%, respectively. The developed hybrid energy storage module can well meet the annual coordination requirements, and has lower levelized cost of electricity. This method provides reasonable reference for designing and optimizing the wind-solar-hydrogen complementary system.

KEYWORDS

wind-solar-hydrogen hybrid system, water electrolysis, fuel cell, fluctuation smoothing, capacity configuration

1 Introduction

The use of fossil fuels has produced a large amount of greenhouse gases, exacerbating global warming and climate change (Temiz and Dincer, 2023). Renewable energy can mitigate the drawbacks of fossil fuels by meeting energy demand requirements, ensuring long-term sustainable production and reducing the negative environmental impacts. Among them, wind and solar are the two most widely used renewable energy power generation technologies. They hold promise as clean and efficient sources of renewable energy,

contributing to achieving net-zero emissions and reducing dependence on fossil fuels (Eltayeb et al., 2023; Ma et al., 2023).

Therefore, the development of wind and solar power generation is crucial for promoting the transformation of energy structure. Nevertheless, the uncertainty and volatility of wind and solar power generation pose significant challenges to the secure operation of power systems (Han et al., 2023; Zhou et al., 2024), and how to alleviate this situation has become a necessary research topic. In this case, storage units become essential, albeit at a higher cost, and more sophisticated wind-solar grid-connected strategies need to be further developed to reduce energy abandonment rates (Das et al., 2022). To address this issue, the researchers proposed an intermediate buffer system to coordinate the supply side and the user side from solar-wind hybrid generation. In order to alleviate the impact of intermittent wind and solar power generation on residential electricity consumption, Tajouo et al. (2023) and Zarate-Perez et al. (2023) proposed a multi-energy complementary system comprising PV/Wind/Battery. Through the real-time load comparison with power generation and energy storage, the integration of an energy storage system extends the full load operation time of the electrolytic cell and reduces the cost of hydrogen production. The flywheel energy storage system is also adopted as an energy storage solution (Erdemir and Dincer, 2020; Amry et al., 2023; Hutchinson and Gladwin, 2023). The implementation of flywheel energy storage holds significant potential in enhancing the Net Present Value, reducing the load capacity, and optimizing the economic benefits. This allows for flexible resource scheduling without compromising the system's economic viability. Liu et al. (2023b) and Nejadian et al. (2023) utilized a wind-solar hybrid hydrogen production system to mitigate fluctuations, enhance resource utilization, and contribute to the standardization strategy of wind-solar hybrid hydrogen production systems. Compared to the other energy storage methods, hydrogen energy storage offers the advantage of versatility across various fields, such as the chemical industry and energy sector, resulting in higher economic benefits (Tang et al., 2022; Kakavand et al., 2023). By combining water electrolytic with wind and solar power generation, the fluctuating power from wind and solar sources is converted into high-quality, high-calorific value green hydrogen. This transformation helps to alleviate the problem of abandoning wind and solar in power generation (Ruhnau, 2022; Prestat, 2023). Moreover, it provides multiple advantages, such as mitigating power fluctuations, ensuring power system stability, and improving market value (Temiz and Dincer, 2022; Superchi et al., 2023).

With the increasing scale of wind and solar power generation, the system complexity, equipment capacity, and initial investment also increase. To achieve the stable operation and enhance the economic efficiency, it is essential to coordinate the capacity configuration optimization and control strategy of the multi-energy complementary system (Zhang and Maleki, 2022; Bai et al., 2023). Liu et al. (2023a) proposed a wind-solar-hydrogen multi-energy supply system integrated with the power grid to distribute the power load, and evaluate the optimization potential for each component of the optimized subsystem using exergy destruction efficiency as an indicator, providing a foundation for subsequent optimization. To optimize the hydrogen load demand and investment costs according to the user requirements, Huang et al. (2023) put forward a day-ahead optimal scheduling strategy based on the principle of aligning energy demand values with the system supply. Compared to the traditional scheduling strategy, the daily profit increased by 12.5%. Liu et al. (2022) introduced a multi-level control method suitable for a wind-solar-storage multi-energy complementary system, enhancing both the stability of the power grid and energy consumption capacity. Through economic analysis of the same optimization target using different control methods, it was found that the new control method significantly reduces the investment cost. Zhang et al. (2023) proposed a system regulation model considering thermal inertia and user comfort, which has a positive impact on the high proportion utilization of renewable energy. Wang et al. (2022) proposed an economic optimal scheduling method with the objective of maximizing system profit, which proves to be highly effective in adapting to the market demand and achieving higher economic benefits. Ibáñez-Rioja et al. (2023) optimized the control method and system capacity based on the minimization of the Levelized Cost of Hydrogen, leading to an increased running time of the electrolytic cell at full load. Balancing economic considerations with enhancements and meeting various scenario requirements, Li et al. (2022) conducted a multi-objective optimization on the capacity configuration and control method of a wind-solar-pumped hybrid storage system to minimize investment costs and maximize system economic benefits. Behzadi and Sadrizadeh (2023) proposed a multi-energy complementary system of wind-solar-hydrogen to optimize the system capacity configuration, reduce the peak capacity and energy cost. The two-way connection with the heating network and power grid enables the system to adequately satisfy the energy demand in the building. Pan et al. (2023) optimized the control method with the goal of minimizing the operating cost of the wind-solar hybrid power generation system. As a result, the integration of a wind-solar power grid system with hydrogen energy storage enhances the utilization efficiency of wind and solar resources, leading to improved economic benefits. It provides a more effective and flexible allocation control scheme, especially when integrating numerous new energy power generation systems, by connecting renewable energy to the grid.

To satisfy the requirements of wind-solar power grid connection, and then enhance the system's stability and economic efficiency, the capacity configuration method of the multi-energy complementary system has been optimized, and thus improved the system control strategy. These enhancements will significantly improve the power supply stability and economic feasibility of the system. Additionally, the fluctuating outputs of solar and wind power impact the frequent start and stop of the electrolyzer in energy storage devices, reducing their lifespan and hydrogen production efficiency. To address these issues and ensure the system's stable operation, this work focuses on constructing a hybrid energy storage module integrating batteries, electrolyzers, and fuel cells. A wind-solar-hydrogen multi-energy complementary grid-connected system has been developed. Furthermore, the influencing factors of alkaline electrolyzers are analyzed, and a grid connection strategy and capacity configuration optimization method are proposed in conjunction with the hybrid energy storage unit. The economic benefits and dynamic performance of the optimized system are further analyzed. The main contributions of this research can be outlined as follows:

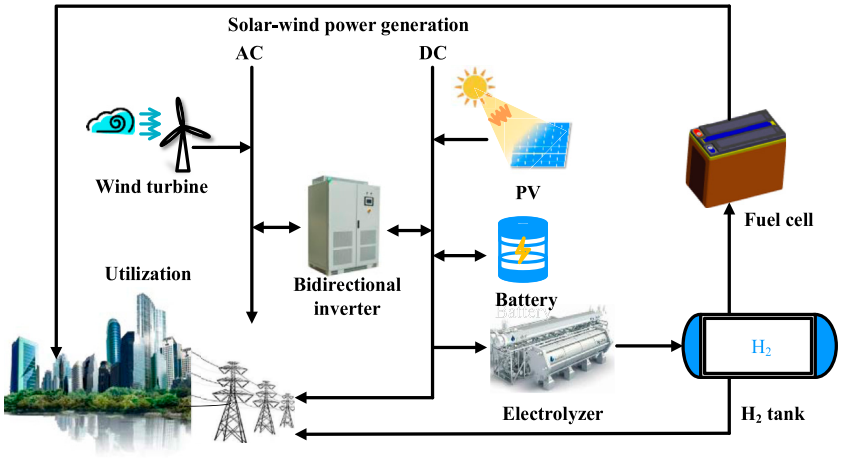

FIGURE 1
Wind-solar hydrogen coupling multi-energy complementary system.

(1) The wind-solar-hydrogen multi-energy complementary system is constructed. A smoothing strategy of power generation grid connection based on sliding average method is proposed, which mitigates the influence of wind-solar power rapid fluctuation. The dynamic process of the system under this strategy is further analyzed.
(2) The alkaline electrolyzer, battery, hydrogen tank and fuel cell equipment are combined to form a hybrid energy storage module. The energy management strategy is further developed, and the module is used to coordinate the grid connection of wind and solar power generation. In addition, the system performance and dynamic operation characteristics are evaluated.
(3) In order to improve the economic benefits of the wind-solar-hydrogen complementary multi-energy complementary system, the capacity configuration optimization model of the system is established. And the differential evolution algorithm is used to optimize the capacity configuration. The system investment construction cost is further analyzed.

The rest of this paper is organized as follows: The process of conceptual and mathematical modeling is introduced in Section 2. The hydrogen production characteristics of alkaline electrolysis cell and the capacity configuration model of wind-solar-hydrogen coupled multi-energy complementary system is established in Section 3. The main results and analysis are presented in Section 4 and the main conclusions are summarized in Section 5.

2 Wind-solar-hydrogen hybrid multi-energy complementary system and model

2.1 Wind-solar-hydrogen hybrid multi-energy complementary system

In order to address the issue of fluctuations caused by the large-scale integration of wind and solar energy into the grid, this study proposes a multi-energy complementary system of wind-solar-hydrogen hybrid by combining wind-solar hybrid power generation, electrolytic water hydrogen production, and fuel cell system. The system's operational process is illustrated in Figure 1. The key equipment of this system includes wind turbines, photovoltaic generators, alkaline electrolyzers, pressure hydrogen storage equipment, battery equipment, and fuel cells.

In the integrated system, wind power generation and photovoltaic power generation serve as the primary power sources. The smoothed power generated is directly fed into the grid for utilization. Excess clean green electricity is stored through battery technology or utilized to drive the alkaline electrolyzer for high-quality hydrogen production, which facilitates chemical energy storage. Moreover, the hydrogen storage equipment and fuel cell are employed as supplementary components for power generation, thereby enhancing the overall stability of the system's operation.

The whole wind-solar-hydrogen hybrid multi-energy complementary grid-connected constitutes an "electricity-gas-electricity" closed-loop structure. The wind and photovoltaic output power are adjusted by the control system to reduce the fluctuation of on-grid power and configure the hydrogen production. The alkaline electrolyzer, hydrogen storage equipment, battery and fuel cell together constitute a hybrid energy storage module. When the proportion of wind and solar power generation in the system exceeds the on-grid power, the module adopts the measures of battery and alkaline electrolytic water hydrogen production to absorb excess wind and solar power generation energy. When the wind and solar power generation power in the system is insufficient, the battery is used to supplement the shortage of wind and solar power generation. When the hydrogen energy storage is sufficient, the fuel cell is used to supplement the shortage to further smooth the system's on-grid power, as shown in Figure 2. In order to achieve the goal of economic operation of the system, it is necessary to optimize the capacity of equipment such as hydrogen production and fuel cell with levelized cost of electricity(LCOE) as the target (Ang et al., 2022).

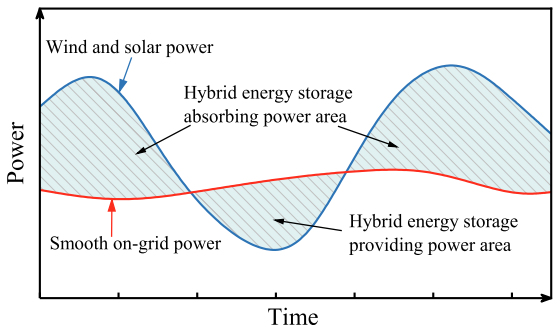

FIGURE 2
Smooth grid connection and shortage supplement schematic diagram.

2.2 Wind-solar hybrid hydrogen system modeling

2.2.1 Wind and solar power output modeling

Wind turbine and photovoltaic array serve as the energy supply components of the multi-energy complementary system. The wind turbine's output power, denoted as P_{WT}, is contingent on the wind speed v, thus wind power exhibits characteristics of fluctuation and intermittency. The wind turbine's output power is calculated as Eq. 1 (Chaichan et al., 2022; Nasrabadi and Korpeh, 2023):

$$P_{WT} = \frac{1}{2}\rho A_{WT} v^3 C_p \tag{1}$$

where ρ is the air density, A_{WT} is the swept area by the rotor and C_p is the coefficient of performance of the wind turbine, respectively.

Photovoltaic array converts the solar radiation into electrical energy based on photoelectric effect, and the photovoltaic output power P_{PV} can be calculated as Eq. 2 (Praveenkumar et al., 2022):

$$P_{PV} = N_{PV}\frac{D}{D_0}\left[\max P_{PV} + \mu\left(T_{PV} - T_a\right)\right] \tag{2}$$

where D and D_0 are actual the solar irradiance and reference solar irradiance, respectively. T_{pv} and T_a are the temperature of PV and ambient temperature, N_{PV} is the number of PV cell units, μ is the temperature coefficient of module efficiency.

2.2.2 Alkaline electrolyzer modeling

As for the electrolyzers, the load power is adapted by adjusting its current, and the temperature-dependent electrode kinetics of the alkaline electrolytic cell stack can be modeled as Eq. 3 (Fang and Liang, 2019):

$$V_{AE} = V_{rev} + \frac{r}{A_{AE}} I_{AE} + s\log\left(\frac{T_{AE}}{A_{AE}} I_{AE} + 1\right) \tag{3}$$

where V_{AE} and V_{rev} are the voltage and reversible voltage, respectively. T_{AE} is the temperature of the electrolyzers, r is the ohmic resistance parameter of the electrolyte, A_{AE} is the effective area of the electrolyzers, and s is the electrode overvoltage coefficients.

The molar rate of hydrogen production n_{H2} is obtained by Eq. 4 (Fang and Liang, 2019):

$$n_{H2} = \eta_F \frac{N_{AE} I_{AE}}{2F} \tag{4}$$

where N_{AE} and I_{AE} represents the number of electrolyzer and electrolyzer current, respectively. F is the Faraday constant of 96487 C/mol.

The electrolysis efficiency η_{AE} is formulated as Eq. 5 (Fang and Liang, 2019):

$$\eta_{AE} = \frac{n_{H2}\Delta G}{P_{AE}} \tag{5}$$

where ΔG is the Gibbs free energy of the electrochemical reaction.

2.2.3 PEMFC modeling

The fuel cell converts the stored hydrogen into electricity to supplement the grid shortage. The output power of fuel cell is mainly affected by its own polarization characteristics, and its output power P_{FC} can be expressed by Eqs. 6–10 (Jia et al., 2009; Li et al., 2021):

$$P_{FC} = N_{FC} I_{FC}\left(V_{nernst} - V_{act} - V_{ohmic} - V_{con}\right) \tag{6}$$

where I_{FC} represents output current of fuel cell and V_{nernst}, V_{act}, V_{onmic} and V_{con} present thermodynamic potential, activation losses, ohmic losses and concentration losses, respectively. N_{FC} is the number of fuel cells.

$$V_{nernst} = \frac{\Delta G}{2F} + \frac{T_{FC}\Delta S_{FC}}{2F} + \frac{RT_{FC}}{2F}\ln\left(\frac{p_{H2}\sqrt{p_{O2}}}{p_{H2O}}\right) \tag{7}$$

$$V_{ohm} = I_{FC} R_{ohm} \tag{8}$$

$$V_{act} = \xi_1 + \xi_2 T_{FC} + \xi_3 T_{FC}\ln B_0 + \xi_4 T_{FC}\ln I_{FC} \tag{9}$$

$$V_{con} = \frac{RT_{FC}}{2F}\ln\left(\frac{\max j_{FC}}{\max j_{FC} - j_{FC}}\right) \tag{10}$$

where T_{FC} is the temperature of fuel cell, R represents the ideal gas constant, p_{H2}, p_{O2} and p_{H2O} are the pressures at the reaction interface. R_{ohm} is the resistance to H^+ flow in the exchange membrane. ξ_1, ξ_2, ξ_3 and ξ_4 are empirical parameters, B_0 represents the oxygen concentration at the cathode gas level, j_{FC} is the current density.

2.2.4 Battery and hydrogen storage modeling

To further enhance the utilization of wind and solar energy, a lithium iron phosphate battery is used as energy storage device. This enables the storage of the excess wind and solar energy power after the hydrogen production, supplementing power during the period of insufficiencies. The capacity of battery $E_{bat}(t)$ at time t can be expressed as Eqs. 11, 12 (Tajouo et al., 2023):

$$E_{bat}(t) = (1-\sigma)E_{bat}(t-1) - \Delta E_{bat}(t) \tag{11}$$

$$\Delta E_{bat}(t) = \begin{cases} P_{bat}\eta_{bat\_out}\Delta t & P_{bat} < 0 \\ P_{bat}\Delta t / \eta_{bat\_in} & P_{bat} > 0 \end{cases} \tag{12}$$

where σ means the self-discharge rate of the battery. η_{bat_in} and η_{bat_out} represents charging efficiency and discharging efficiency, respectively. $P_{bat}(t)$ is the power of the battery. When $P_{bat}(t) > 0$ the battery will be charged. Conversely, the then battery will be discharged when $P_{bat}(t) < 0$.

Moreover, the inclusion of hydrogen storage equipment is crucial to enhance the stability of hydrogen transportation. Gaseous high-pressure hydrogen storage technology is primarily

TABLE 1 Key parameters used for the modeling of the hydrogen system.

Component	Parameter	Value
Wind turbine	Single rated power	2000 kW
	Inflow wind speed	3 m/s
	Rated wind speed	12.5 m/s
	Outflow wind speed	25 m/s
	Mounting height	80 m
Photovoltaic panel	Single rated power	350 W
	Peak voltage	34.2 V
	Peak current	9.96 A
	Open-circuit voltage	41.7 V
	Short-circuit current	10.55 A
Alkaline electrolyzer	Single rated power	2000 kW
	Single rated hydrogen capacity	400 Nm^3/h
	Hydrogen power operating range	15%–100% Capacity
PEMFC	Single rated power	1,000 kW
	Numbers of cells in series	48
Battery	The range of SOC	0.15–0.9
	Charge and discharge efficiency	98%
Hydrogen storage	Storage pressure range	0.2–5 MPa
	Storage temperature	25°C

employed for short-term storage of hydrogen, ensuring efficient and reliable operation. According to the Clapeyron equation, the state of the tank can be obtained by Eq. 13.

$$\begin{cases} Q_{HT}(t_0+\Delta t) = \int_{t_0}^{t_0+\Delta t} n_{HT}(t)dt + Q_{HT}(t_0) \\ p_{HT}Q_{HT} = RT_{HT}n_{HT} \times 10^{-6} \end{cases} \quad (13)$$

where p_{HT} and Q_{HT} are the pressure and volume of the hydrogen storage tank, respectively. n_{HT} is the hydrogen molar amount. T_{HT} is the thermodynamic temperature of hydrogen storage, and R represents the ideal gas constant.

In the wind-solar hybrid hydrogen production system, the key parameters of the main equipment are presented in Table 1 (Su et al., 2023).

3 Capacity configuration method of wind-solar hybrid multi-energy complementary system

In the multi-energy complementary system of wind-solar-hydrogen hybrid, the alkaline electrolyzer plays a crucial role in the hybrid energy storage module. Its operational characteristics and dynamic behavior directly impact the stabilization characteristics of the entire multi-energy complementary system. Additionally, the scheduling strategy and capacity configuration method employed in the system also have significant effects on the operation cost of the entire system.

3.1 Operating characteristics of alkaline electrolyzer for hydrogen production

The alkaline electrolyzer, battery, hydrogen storage tank and PEMFC constitute the energy storage and consumption link of the multi-energy complementary system of wind-solar-hydrogen coupling. The battery is used as an electrochemical energy storage device, which has the characteristics of fast cycle speed and low cycle life, while the corresponding speed of PEMFC is milliseconds to seconds, both of them can adapt to the rapid fluctuation of power. In contrast, the alkaline electrolyzer has a slower response speed and a certain lag, and its operating state will greatly affect the operating state of the hybrid energy storage module. This work will mainly analyze the operation characteristics of alkaline electrolyzer in wind and solar power generation. The analysis holds great significance in formulating a coordinated grid-connected operation strategy for the system and enhancing its overall stability.

In the wind-solar power generation hydrogen production system, the wind-solar power as the power input source, which will affect the hydrogen production process of electrolytic water. External environmental conditions, such as wind speed, radiation intensity and other factors affecting wind and solar power generation power, indirectly affect the rate of hydrogen production from electrolytic water. In addition to the indirect factors, the hydrogen production rate of alkaline electrolyzer is also affected by the working current, working temperature and operating characteristics. The operating characteristics of alkaline electrolyzer in the actual operation process are as follows:

(1) Working fluctuation characteristics: Electrolyzers can operate efficiently within a range of 15%–100% of their nominal capacity (Lüke and Zschocke, 2020). Within this range, the electrolyzer offers fine-grained power regulation capabilities. Operating the electrolyzer below 15% of its rated power for an extended period can lead to the risk of explosion in the electrolytic cell. Conversely, operating the electrolyzer at a current density higher than the rated current density can cause damage to the stack material. Consequently, the minimum rated power of 15% is a critical specification adhered to by most manufacturers.
(2) Start-stop characteristics: At this time, the alkaline electrolyzer is in a long-term non-working state, consuming no power and ceasing hydrogen production. Upon restarting, power consumption is initially directed towards raising the temperature of the alkaline electrolyzer since it may not be sufficiently high to initiate hydrogen production (Ulleberg et al., 2010).
(3) Thermal insulation characteristics: During the shutdown of the alkaline electrolyzer, an environmental control device is employed to maintain the cell's temperature within a specific range, ensuring that hydrogen production requirements can still be met. Under this state, provided that the fluctuating power supply is replenished promptly, the alkaline electrolyzer can

resume operation within a certain period after being shut down (Shen et al., 2018).

Hence, based on the operating characteristics of the alkaline electrolyzer, a sensitivity analysis of the working current and working temperature will be conducted to simulate and analyze the dynamic operation of hydrogen production through electrolytic water under fluctuating power conditions. Additionally, during practical operation, utmost emphasis will be placed on ensuring the safety and stability of the electrolyzer, enabling it to operate efficiently even under varying loads.

3.2 Control strategy of wind-solar-hydrogen coupling multi-energy complementary system

3.2.1 Wind-solar power generation grid-connected smoothing strategy

In this paper, the sliding average method is used to smooth the output power of wind and solar power and improve the utilization rate of these renewable energy resources. Through the meteorological prediction parameters of wind speed and radiation, the wind and solar power generation model is used to calculate the wind and solar power generation power, and the grid-connected power is further smoothed by the sliding average method. The basic principle is to smooth the data by calculating the average value of the data in a certain window. The expression is expressed as Eq. 14

$$P_{\text{gird}}(t) = \frac{1}{l}\sum_{t_1=t-(N/2-1)}^{t+N/2}\left(P_{\text{WT}}(t_1) + P_{\text{PV}}(t_1)\right) \tag{14}$$

where P_{grid} is the grid-connected power, and l is the window scale, which is the important parameter of the moving average method. The larger the value is, the smoother the grid-connected power is. If the window scale is too large, a higher energy storage system needs to be configured. If the window scale is too small, it cannot meet the grid-connected requirements.

By employing the maximum fluctuation rate as a measure of the peak-valley difference in power fluctuations, one can systematically determine an appropriate window scale. Additionally, to comprehensively capture the overall dynamics of power fluctuations, output standard deviation (Eq. 15) and maximum fluctuation rate (Eq. 16) will be utilized as indicators to evaluate the effectiveness of power fluctuation (Ren et al., 2023).

$$d = \frac{1}{P_{\max}}\sqrt{\frac{1}{N}\sum_{t=1}^{N}\left(P_t - \bar{P}\right)^2} \tag{15}$$

where d is the standard deviation of output, the smaller the standard deviation, the smaller the fluctuation of wind power. $P_{\max}$ presents the maximum operating power.

$$k_{\max} = \frac{|P_t - P_{t-1}|}{P_{\max}} \times 100\% \tag{16}$$

where $k_{\max}$ is the maximum fluctuation rate, which reflect the maximum fluctuation of wind and solar power.

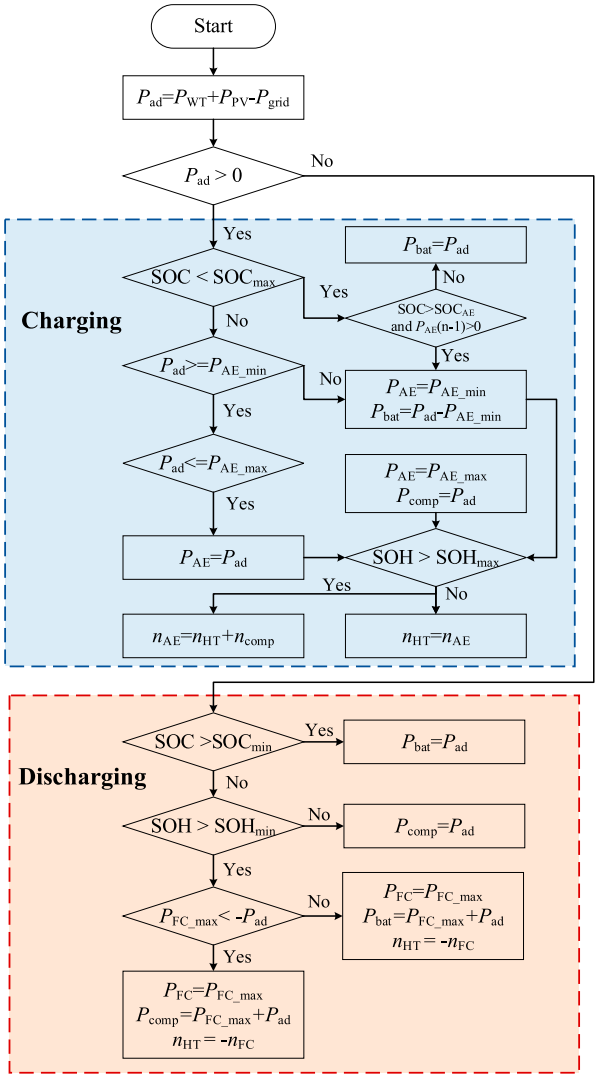

FIGURE 3
Diagram of energy management strategy for hybrid energy storage module.

As a result, by setting the grid-connected power fluctuation within a 10-min time interval as a constraint, the minimum window scale that adheres to the specified fluctuation limit will be identified. Subsequently, the grid-connected power of wind-solar power generation will be calculated using this minimum window scale. Any disparities between the grid-connected power and the actual power generated by wind-solar sources will be managed and balanced through the utilization of a hybrid energy storage module. This approach ensures efficient coordination and management of the power fluctuations, contributing to a stable and reliable grid-connected power system.

3.2.2 Energy management strategy of hybrid energy storage mode

In this hybrid energy storage module, both the battery and PEMFC are capable of achieving rapid power regulation, while the alkaline electrolyzer can perform large-scale power regulation at a minute level. However, the electrolyzer should not be operated at low power levels for extended durations. With the objective of ensuring the operational

range of each device, this strategy utilizes the state of charge (SOC) of the battery reserve as a crucial benchmark for power regulation. At the same time, due to the different power between the wind-solar and the grid-connected at each moment, the charging and discharging state of the hybrid energy storage module can be reflected. The difference charging state(P_{ad}) is combined with the SOC of battery to form the following operating mode, as shown in Figure 3.

Mode 1: When the hybrid energy storage is in the charging state ($P_{ad} > 0$), the excess power after grid-connected is stored by the battery and the electrolytic cell:

(1) When the module meets the following conditions, as expressed by Eq. 17:

$$\begin{cases} P_{ad} > 0 \\ \mathrm{SOC} < \mathrm{SOC}_{max} \end{cases} \tag{17}$$

There is an excess margin of the battery, which will be stored through the battery.

(2) When the module meets the following conditions, as expressed by Eq. 18 the electrolytic cell is mainly used for hydrogen production to convert electrical energy into chemical energy:

$$\begin{cases} P_{ad} > 0 \\ \mathrm{SOC} \geq \mathrm{SOC}_{max} \end{cases} \tag{18}$$

The battery has no excess energy storage, so the electrolyter works. When P_{ad} does not meet the minimum hydrogen production power, the battery will be supplemented to meet its minimum operation and less outage time. When P_{ad} is in the power range of the electrolyzer will be used for normal hydrogen production, and the hydrogen will be stored in the hydrogen storage tank, and the excess hydrogen can be transported as a product. In addition, the power exceeding the working range of the electrolyzer will be discarded.

Due to the operating characteristics of the alkaline electrolyzer, it requires a certain time for restarting up. To enhance its operation duration, the SOC_{AE} is established within the SOC operating interval. When the alkaline electrolyzer is in operation and the SOC is more than the SOC_{AE}, because of the battery storing sufficient power, the P_{ad} and battery supply power to ensure the lowest power operation. However, when the SOC is less than SOC_{AE}, the alkaline electrolyzer ceases operation to prevent rapid shutdown.

Mode 2: When the hybrid energy storage is in the discharge state ($P_{ad} < 0$), the battery and PEMFC in the hybrid energy storage module are needed to supplement:

(1) When the module meets the following conditions, as expressed by Eq. 19:

$$\begin{cases} P_{ad} < 0 \\ \mathrm{SOC} > \mathrm{SOC}_{min} \end{cases} \tag{19}$$

Under this condition, the battery has enough power to supplement the shortage, and thus, the shortfall is directly supplemented through battery discharge.

(2) When the module meets the following conditions, as provided in Eq. 20 the PEMFC is mainly used to consume hydrogen to generate electricity to supplement the shortage:

$$\begin{cases} P_{ad} < 0 \\ \mathrm{SOC} \leq \mathrm{SOC}_{min} \end{cases} \tag{20}$$

In this situation, the battery no longer supplements the shortage, and the PEMFC starts consuming the hydrogen from the hydrogen storage tank for discharge. If the hydrogen level of the tank falls below the minimum value, the PEMFC will shut down without consuming hydrogen any more, and alternative flexible resources will be scheduled for compensation. However, when the quantity of hydrogen in the tank is sufficient, the PEMFC will operate at rated power and prioritize the power supply to grid. If the power supply is insufficient, other resources will be utilized to compensate. Conversely, if the power supply is sufficient, the excess power will be directed to charge the battery.

By implementing the above energy management strategy, effective coordination among the battery, alkaline electrolyzer, hydrogen storage tank, and PEMFC will be achieved, enabling a seamless grid connection of wind and solar power generation. And setting the state condition of SOC_{AE}, it provides a buffer for the running of the electrolyzer and improves coordination. In addition, compared with conventional energy storage, the adopted hybrid energy storage is also conducive to reducing the total scale of energy storage capacity.

3.3 Capacity configuration optimization model of wind-solar-hydrogen coupling multi-energy complementary system

Based on the grid-connected smoothing strategy of wind-solar power generation and the energy management strategy of hybrid energy storage module, the capacity configuration optimization model of multi-energy complementary system with wind-solar-hydrogen coupling is further established to improve the economy of the system.

3.3.1 Objective function and decision variables

The *LCOE* of the multi-energy complementary system is used as the optimization objective function, and the alkaline electrolyzer, battery, fuel cell and hydrogen storage are used as decision variables to optimize the capacity configuration of the equipment by minimizing the LCOE. The objective function is expressed as Eq. 21 (Sultan et al., 2023):

$$LCOE = \frac{C_{inv} - \frac{RS}{(1+i)^L} + \sum_{y=1}^{L}\left(\frac{C_{O\&M}+C_{comp}-c_{H_2}M_{H_2}}{(1+f)^y/(1+i)^y}\right)}{\sum_{y=1}^{L}\left(P_{grid}\Delta t\right)} \tag{21}$$

where *RS* is the scrap value of fixed assets, *L* is the lifetime, *f* is the inflation rate, and *i* is the interest rate 8%. M_{H2} is the mass of hydrogen production, c_{H2} is the unit hydrogen price. C_{inv} is the total investment cost of each equipment. $C_{O\&M}$ is the total operating cost of each equipment, and C_{comp} is the additional power supplement cost. The equipment investment cost and operation and maintenance cost corresponding to each equipment are shown in Table 2 (Buttler and Spliethoff, 2018; Dowling et al., 2020; Zhao et al., 2022; Al-Ghussain et al., 2023; Han et al., 2023).

TABLE 2 Cost of the main components for wind-solar power and electrolysis.

Equipment	Capital cost	Operation cost	Lifetime
Group PV	540 $/kW	6 $/kW/y	30
Wind turbine	825 $/kW	15.73 $/kW/y	20
Alkaline electrolyzer	657 $/kW	2% Capital cost	20
Battery	261 $/kWh	0.004 $/kWh/h	10
Fuel cell	2400 $/kW	2% Capital cost	20
Hydrogen tank	575 $/m^3	2% Capital cost	20

(1) The investment cost includes the initial investment in wind power generation equipment, photovoltaic arrays, alkaline electrolyzers, batteries and fuel cells, which can be calculated by Eq. 22:

$$C_{inv} = c_{inv\_WT}E_{WT} + c_{inv\_PV}E_{PV} + c_{inv\_AE}E_{AE} + c_{inv\_bat}E_{bat} + c_{inv\_FC}E_{FC} + c_{inv\_HT}E_{HT} \quad (22)$$

where c_{inv} is the unit equipment purchase cost of each equipment, and E is the total capacity of each equipment.

(2) The operation and maintenance is the sum of the operation and maintenance cost of each equipment in the system life cycle, which can be calculated as Eq. 23:

$$C_{O\&M} = c_{O\&M\_WT}E_{WT} + c_{O\&M\_PV}E_{PV} + c_{O\&M\_AE}E_{AE} + c_{O\&M\_bat}E_{bat} + c_{O\&M\_FC}E_{FC} + c_{O\&M\_HT}E_{HT} \quad (23)$$

where $c_{O\&M}$ is the unit operation and maintenance cost of each equipment, and E is the total capacity of each equipment.

(3) The additional power compensation cost can be calculated as Eq. 24:

$$C_{comp} = c_{comp}P_{comp} \quad (24)$$

In addition, *IRR* is used to evaluate the economic characteristics of the system, with the expression of as Eq. 25 (Meng et al., 2023):

$$\sum_{y=1}^{L}(C_{in} - C_{cost})_y(1 + IRR)^{-y} = 0 \quad (25)$$

where C_{in} and C_{cost} are the revenue and expenditure of the system in year y, respectively.

3.3.2 Constraint condition

During system operation, the wind-solar-hydrogen coupling multi-energy complementary system must prioritize safe and stable operation, which necessitates the implementation of certain constraints.

(1) Power balance constraint. The dynamic operation of the system satisfies the energy conservation constraint, that is, the difference between the wind-solar complementary output power generation and the grid-connected power is adjusted by the hybrid energy storage module, which can be expressed as Eq. 26:

$$P_{WT} + P_{PV} - P_{grid} = P_{AE} + P_{bat} + P_{FC} + P_{comp} \quad (26)$$

(2) Equipment operation constraints. Alkaline electrolyzer and fuel cell operating power should be within the allowable range, with the power constraints being expressed as Eq. 27:

$$\begin{cases} \min P_{AE} \le P_{AE} \le \max P_{AE} \\ \min P_{FC} \le P_{FC} \le \max P_{FC} \end{cases} \quad (27)$$

(3) Energy storage and hydrogen storage constraints. The battery and hydrogen storage tank, serving as energy storage and hydrogen storage equipment, need to be constrained within a certain reserve range due to safety limitations. The formulation is Eqs. 28, 29:

$$\min SOC \le SOC \le \max SOC \quad (28)$$

$$\min SOH \le SOC \le \max SOH \quad (29)$$

where SOC is the battery state of charge, SOH is the state of hydrogen tank.

(4) The on-grid power of wind-solar power generation should be guaranteed within a safe range. The formulation is Eq. 30:

$$\begin{cases} \Delta P_{grid\_10} \le 10, & (E_{WT} + E_{PV}) < 30 \\ \Delta P_{grid\_10} \le (E_{WT} + E_{PV})/3, & 30 \le (E_{WT} + E_{PV}) \le 150 \\ \Delta P_{grid\_10} \le 50, & (E_{WT} + E_{PV}) > 150 \end{cases} \quad (30)$$

where ΔP_{grid_10} is the difference of on-grid power at a 10-min interval. (E_{WT}+E_{PV}) is the installed scale of wind-solar power generation, with the unit of megawatt.

4 Results and discussion

This section conducts an in-depth analysis of the capacity configuration and dynamic operation of the wind-solar-hydrogen coupling multi-energy complementary system, incorporating the operation strategy and capacity configuration optimization method. Specific application cases are examined to analyze the influencing factors of hydrogen production in alkaline electrolyzers. This analysis will lead to further optimization of the capacity configuration for each device, followed by a comprehensive investigation into the dynamic operation characteristics of the system.

4.1 Operating characteristics analysis of alkaline electrolyzer

In the wind-solar-hydrogen coupling multi-energy complementary system, the process of hydrogen production through water electrolysis with the alkaline electrolyzer is subject to various influencing factors, including equipment parameters, power fluctuations, and environmental conditions. The influence of equipment parameters on its operating state is first examined. Figure 4 illustrates the relationship between the working voltage, working power, and input current of a single alkaline electrolyzer. As the temperature of electrolyzer increases, the working voltage of the

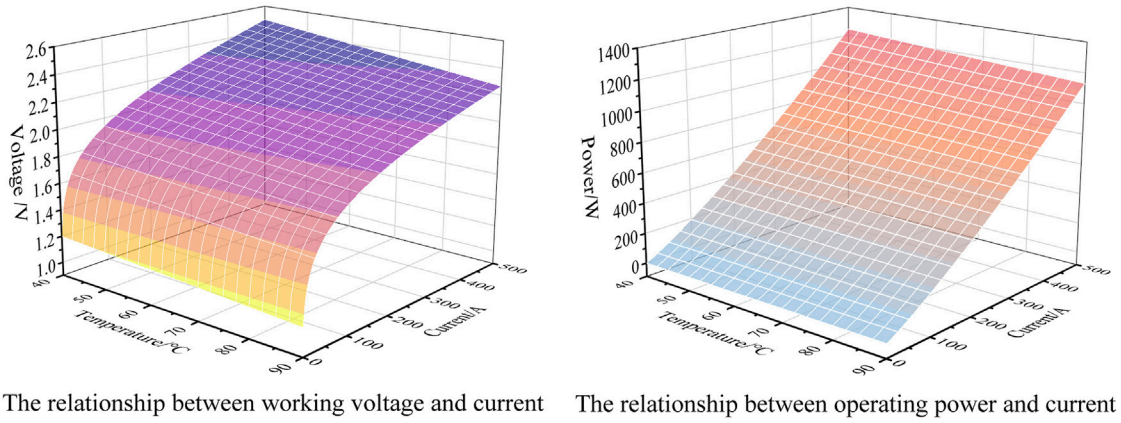

FIGURE 4
The relationship between current and voltage and current at different temperatures.

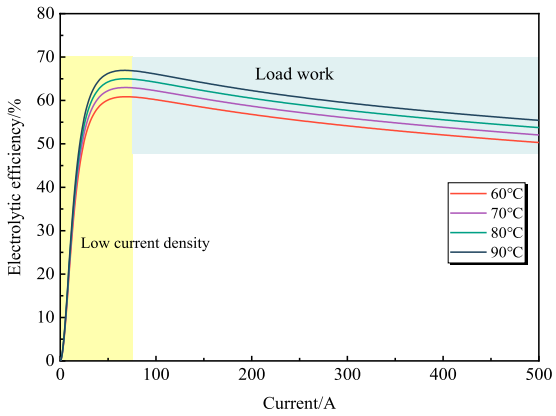

FIGURE 5
Relationship between electrolysis efficiency and current in different temperatures.

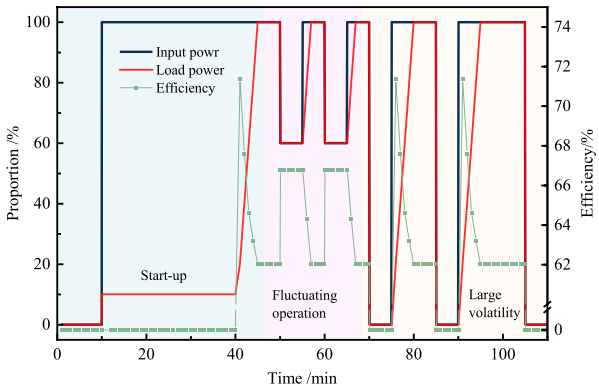

FIGURE 6
The operating state diagram of the electrolytic cell under simulated fluctuating power.

electrolyzer gradually decreases due to the activation of the electrolysis catalyst. Meanwhile, with the increase in current density, the voltage gradually increases, indicating that the electrolyzer is non-linear resistive. Moreover, the power of the electrolyzer also decreases with the increasing temperature. It can be seen that an appropriate increase in temperature is conducive to alkaline electrolysis water hydrogen production.

Figure 5 depicts the relationship between electrolysis efficiency and current in different temperatures. It shows that there is a clear correlation between the state of the alkaline electrolytic cell and the input current. The electrolytic cell efficiency initially increases with rising current. When the current reaches 70 A, the efficiency decreases after reaching the peak, furthermore, both of the maximum efficiency of the electrolytic cell and the corresponding current rise with the increasing working temperature. At lower current density, the working temperature exerts minimal influence on the electrolysis efficiency, while the efficiency increases with increasing temperature at the work load conditions.

During the stable operation period, the continuous operation of the electrolytic cell at a predetermined temperature and rated power level can be ensured by accurately adjusting the input current. However, when the current input to the electrolyzer fluctuates, the electrolyzer cannot be guaranteed to operate continuously within the optimal operating rang, which will directly affect the hydrogen production efficiency and stability of the system. As depicted in Figure 6, the input fluctuation power supply is used to simulate different states of the electrolytic cell, including start-up, normal fluctuation states and large volatility fluctuation states. After an initial 10-min shutdown, the electrolyzer experiences a start-up lag of more than 30 min before commencing hydrogen production. When the electrolytic cell reaches the rated working state, the load power further increased resulting in an increase in temperature and a decrease in electrolysis efficiency. Subsequently, the load power remains stable at the rated operating condition, resulting in an energy loss of 82.6% throughout this process. At the 50 min, the input power enters in a fluctuating state. During the periods of decreased input power, the load power of the electrolyzer also decreases, affecting

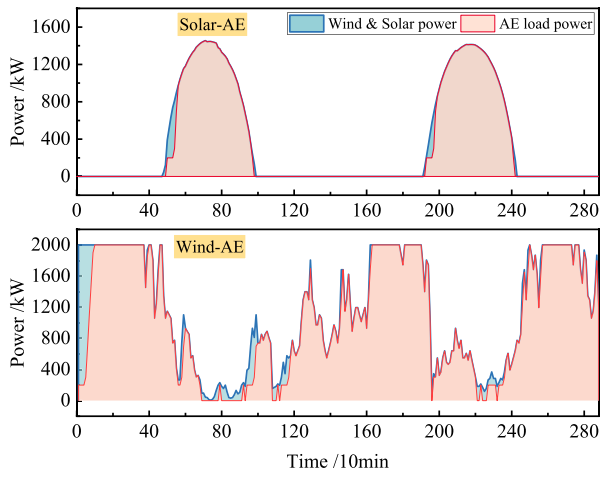

FIGURE 7
Two consecutive days of wind-solar power generation and electrolytic cell load power in Jilin Province, China.

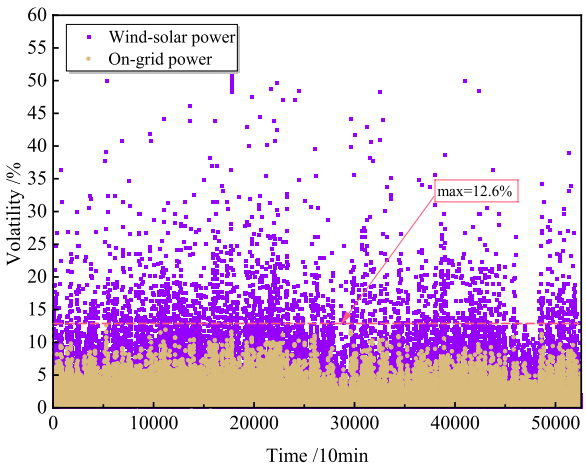

FIGURE 8
The maximum fluctuation rate of 10 min before and after wind and solar power smoothing.

the reaction speed. During this period, the load power of the electrolyzer performs similar to the input power. While at the increasing periods of the input power, the load power exists a slight lag affected by reaction speed. At the 70 min, the input power reaches 0, causing the cell to shut down and electrolytic efficiency decrease to 0. About 5 min later, the input power returns to the rated power while the load power gradually increases according to the limits of the power regulation speed without experiencing another start-up time. The energy loss of the process is reduced to 20.7%, indicating that the short-term shutdown of the electrolytic cell is beneficial for the recovery of working power due to its thermal insulation characteristics.

In the practical operational scenario, the power fluctuations of wind and photovoltaic power generation are more complex compared to the simulated fluctuating power in the previous case. A two-day dataset with a time resolution of 10 min was further simulated for a specific area in Jilin Province, China. The installed capacity of both wind and photovoltaic power systems is set as 2 MW, and the installed capacity of alkaline electrolyzer is 2 MW as well. The simulation results are presented in Figure 7. In the investigated situation, the photovoltaic system operates solely during the daytime, while the wind turbine operates throughout the day, and its power generation at night is higher. Additionally, the volatility of wind power generation is more pronounced compared to photovoltaic power generation. Photovoltaic hydrogen production experiences only a slight lag during the start of photovoltaic power generation. However, wind power exhibits frequent fluctuations, with the maximum volatility reaching as high as 47.2%. Consequently, the lag of the electrolytic cell in response to wind fluctuations is more significant. Overall, the simulation results indicate that wind power has a more substantial impact on the hydrogen production of the electrolytic cell when compared to photovoltaic power generation. The frequent and larger fluctuations in wind power pose greater challenges for maintaining stable hydrogen production in the electrolytic cell.

4.2 Capacity configuration optimization of multi-energy complementary system

The large-scale application scenarios of the capacity configuration method of wind-solar-hydrogen coupling multi-energy complementary system are studied. The analysis will cover a total time scale of 1 year, and the case will involve an installed capacity of 150 MW for both wind and photovoltaic power systems. Considering the standard of grid-connected power, a maximum fluctuation rate limit of 16.7% for a 10-min interval is imposed. To satisfy this limit, the approach involves increasing the window scale for calculating fluctuations. Through this method, it is observed that when the window scale is set to 4, the maximum fluctuation rate for a 10-min time interval reduces to 12.6% (after smoothing) from 51.3% (before smoothing), resulting in a substantial reduction of 38.7%. This improvement of the maximum fluctuation rates after smoothing is shown in Figure 8. Due to the application of the smoothing technique, the grid-connected power fluctuations can achieve the required standards, effectively achieving control over grid-connected power fluctuations using the sliding average method.

Further the particle swarm optimization algorithm is used to optimize the minimization of *LCOE*. It's configured with a particle swarm size of 100 and a total of 80 iterations. the capacity configuration optimization results and system costs of each device can be obtained, as presented in Table 3. The final optimization results show that the LCOE is 0.0324 $/kWh, and the total investment cost is 233.3 million dollars. Additionally, there is an extra power compensation cost of 1.167 million dollars due to the limitation of the hybrid energy storage module in stabilizing the entire power output.

Under this capacity configuration scale, hybrid energy storage equipment accounts for 8.3% of the scale of wind and solar construction. In addition, the proportion of initial investment on wind power generation, photovoltaic power generation, electrolytic cell, battery, PEMFC, hydrogen storage tank and other equipment is shown in Figure 9. Among them, wind turbines and photovoltaic

TABLE 3 System capacity configuration optimization results.

Type	Parameter	Value
Capacity configuration	Wind turbine	150 MW
	Photovoltaic	150 MW
	Alkaline electrolyzer	6080 kW
	Fuel cell	5866 kW
	Battery	13174 kWh
	Hydrogen tank	320 m^3
Economic cost	capitalized cost	226.4 million $
	operation and maintenance cost	4.0 million $
	power compensation cost	1.2 million $
	total cost	231.6 million $
	LCOE	0.0324 $/kWh

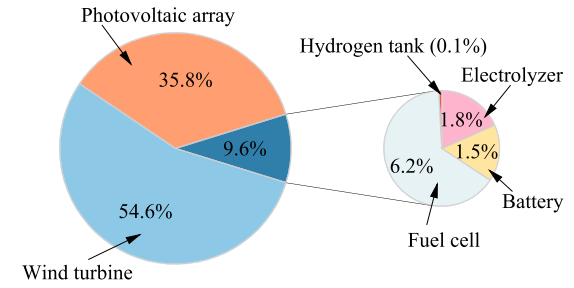

FIGURE 9
The proportion of initial investment cost of each equipment.

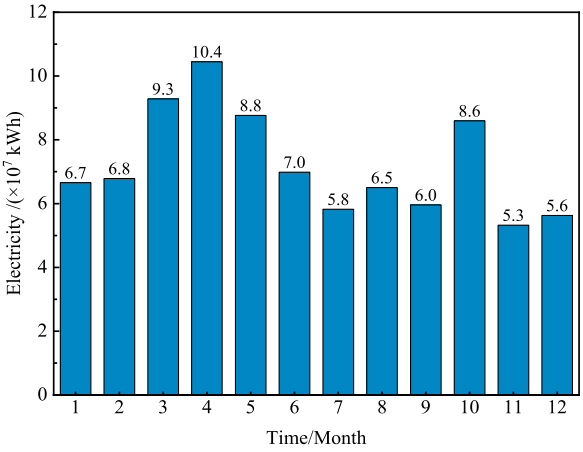

FIGURE 10
The grid-connected amount of wind and solar power generation in each month of the year.

generators are the main power generation equipment, and their purchase costs account for the highest proportion, which is 54.6% and 35.8% respectively. After wind and solar power generation, most of the power is used for grid-connected utilization, so their investment accounts for the largest proportion. For the hybrid energy storage module, the single-machine construction cost of FC is high, so the initial investment cost is the highest. Compared with it, the cost of the battery is lower, but its service life is also shorter (10 years). In the middle of the life of the multi-energy complementary system, a batch of battery equipment needs to be replaced, and its total investment is higher.

Wind-solar power integration serves as the primary means to reap the benefits of the system. The system achieves an annual grid-connected amount of 867.5 million kWh. The monthly grid-connected power generation volumes are illustrated in Figure 10, with the highest grid-connected power occurring in April at 104 million kWh, and the lowest in November at 53 million kWh. This data indicates that the grid-connected volume is lower during winter months, while it is higher in spring and summer. On average, the monthly grid-connected power for the year amounts to 72 million kWh. Considering the current LCOE of 0.0324 $/kWh, setting the electricity price at 0.04 $/kWh allows for an economic analysis. The internal rate of return (IRR) is calculated to be 13.67%, demonstrating the system's favorable economic performance. This positive IRR reflects the economic feasibility of the multi-energy complementary system.

4.3 Operation analysis of wind-solar-hydrogen coupling multi-energy complementary system

Through the above capacity configuration of the multi-energy complementary system of wind-solar-hydrogen coupling, the scale of hybrid energy storage equipment under the total installed capacity of 300 MW is obtained. This section further analyzes the system operation process. This strategy first divides the wind and solar power generation power into two parts by the moving average method, namely, the wind and solar grid-connected power and the hybrid energy storage coordinated power, as shown in Figure 11. The annual real-time wind-solar grid-connected power is relatively smooth, and the standard deviation is reduced to 22.63%. The fluctuation rate of the hybrid energy storage regulation power is significantly low, with the maximum value of 60.0%. It is difficult for the battery, alkaline electrolytic cell, fuel cell and other equipment in the hybrid energy storage module to coordinate excessive power fluctuations, for the module mainly coordinates the power in the range of [-16,16] MW. Moreover, the proportion of data points distributed in this range is 90.3%. Therefore, the module can meet the power smoothing situation in most cases, and the annual coordinated power accounts for 80.5% of the total volume. The additional missing power can be supplemented by other flexible power sources, ensuring good coordination of the system.

As shown in Figure 12, two consecutive days are selected to analyze the operation of each device of the multi-energy complementary system. From the actual operating power of each device, the energy storage device plays a crucial role as the main adjustment mechanism. However, the power fluctuation requiring adjustment exceeds the limit of the hybrid energy storage's capabilities. When the compensating power is negative, power

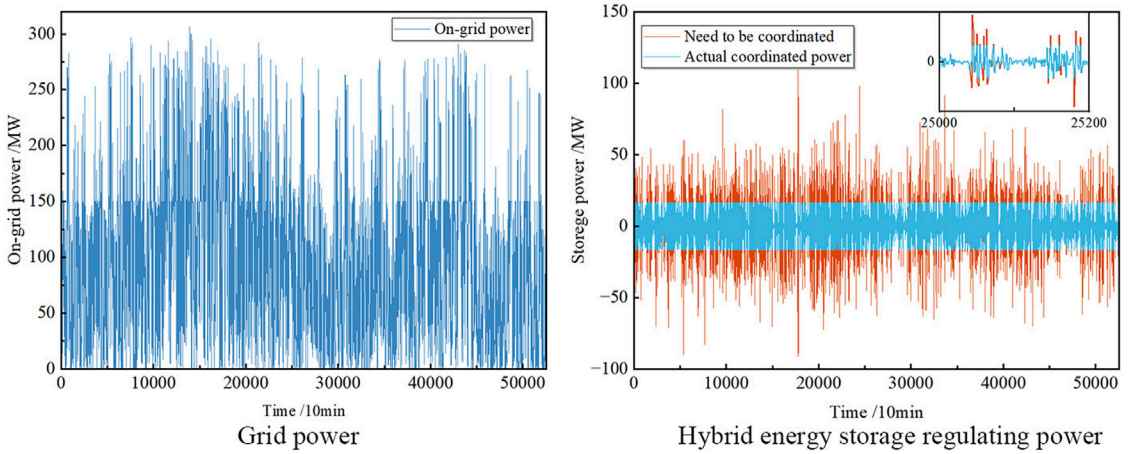

FIGURE 11
Real-time grid-connected power and hybrid energy storage adjustment power throughout the year.

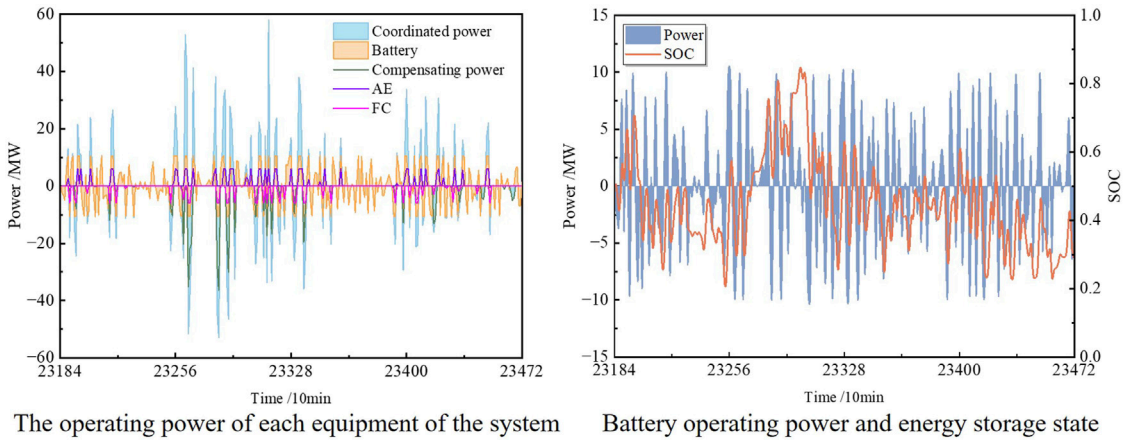

FIGURE 12
Operation of each equipment of multi-energy complementary system.

needs to be supplied to the grid. Batteries and fuel cells can guarantee most of the power supply, while coordinated power adjustments are necessary to regulate the remaining fluctuations. This ensures the safety of electricity consumption and meets the requirements for adjusting grid-connected power. On the other hand, when the compensating power is positive, the battery remains the primary regulating device, with the alkaline electrolyzer coordinating. However, when the power generation exceeds the system storage, the excess part will be wasted.

In contrast, the electrolyzer and fuel cell regulate electricity through the generation and utilization of hydrogen, serving as auxiliary devices. During their operation, they exhibit lower volatility and there are instances of equipment standby. And hydrogen energy serves as a form of energy storage, it enables prolonged energy storage. Moreover, during power supplementation, the fuel cell facilitates rapid replenishment. Due to the relatively slow response of the alkaline electrolyzer, it exhibits lower operational volatility compared to the fuel cell, and there is a lag in hydrogen production. However, by integrating energy storage devices such as the electrolyzer, fuel cell, and battery, the fluctuation in wind and solar power output can be effectively reduced, and the total energy storage capacity is also lower.

In order to ensure the stable operation of the system, it is necessary to understand the working environment of the battery. Therefore, real-time charge and discharge power and the energy storage SOC of the battery are further analyzed and summarized in Figure 12. From the data, it is evident that the battery meets the adjustment requirements within its operating range and undergoes frequent charging and discharging cycles. Additionally, the SOC of the battery is maintained between 0.2 and 0.8, effectively avoiding overcharging and overdischarging, which can be detrimental to the battery's lifespan. In summary, although the hybrid energy storage module cannot fully coordinate all the power fluctuations, it satisfactorily meets the coordination requirements for most of the electricity throughout the year. The battery's operation ensures good regulation within its designed operating range. Furthermore, the use

of power compensation facilitates stable and safe electricity consumption, contributing to the overall efficient operation of the multi-energy complementary system.

5 Conclusion

The study primarily focuses on power grid smoothing, operation strategy and capacity configuration optimization of hybrid energy storage modules for large-scale wind and solar power grid-connected scenarios. The main conclusions can be summarized as follows:

(1) The operating state and hydrogen production efficiency of the alkaline electrolyzer are influenced by the current density and operation temperature. Fluctuating power supplies have a significant impact on the electrolytic cell, leading to energy losses during start-up to the rated state (82.6%) because of the power adjustment speed limits (20.7%). In the practical operation, frequent wind fluctuations exacerbate the lag of the electrolytic cell.
(2) The study employs the sliding average method to reduce the grid-connected power fluctuations of wind and solar power generation. Through capacity configuration optimization, with an LCOE of 0.0324 $/kWh, the hybrid energy storage module accounts for 8.3% of the wind-solar system's total capacity, with a total cost of 233.2 million dollars. The annual grid-connected capacity reaches 8.7 million kWh.
(3) By employing the wind-solar-hydrogen hybrid multi-energy complementary system and the control strategy, real-time annual wind-solar power can smoothly connect to the grid with the standard deviation reduction of 22.63%. The hybrid energy storage module can achieve majority coordination requirements, with annual coordinated power accounting for 80.5% of the total and covering 90.3% of the time period.

This study proposed a grid-connected smoothing strategy and capacity configuration optimization method of the wind-light-hydrogen coupled multi-energy complementary system. It offers technical and methodological suggestions and reference for the formulation of wind-solar hydrogen production scheme with excellent overall performance.

Data availability statement

The raw data supporting the conclusion of this article will be made available by the authors, without undue reservation.

Author contributions

WS: Conceptualization, Investigation, Writing–original draft. QL: Investigation, Visualization, Writing–original draft. SW: Formal Analysis, Investigation, Visualization, Writing–original draft. WZ: Formal Analysis, Investigation, Writing–review and editing. ZB: Investigation, Writing–review and editing. YH: Investigation, Software, Writing–original draft. ZY: Investigation, Software, Writing–review and editing.

Funding

The author(s) declare financial support was received for the research, authorship, and/or publication of this article. The authors appreciate the financial support provided by Shandong Provincial Natural Science Foundation of China (ZR2022YQ58), and the Fundamental Research Funds for the Central Universities (No. 22CX07006A).

Conflict of interest

Authors WS, WZ, and ZY were employed by Powerchina HuaDong Engineering Corporation Limited.

The remaining authors declare that the research was conducted in the absence of any commercial or financial relationships that could be construed as a potential conflict of interest.

Publisher's note

References

Al-Ghussain, L., Ahmad, A. D., Abubaker, A. M., Hovi, K., Hassan, M. A., and Annuk, A. (2023). Techno-economic feasibility of hybrid PV/wind/battery/thermal storage trigeneration system: toward 100% energy independency and green hydrogen production. *Energy Rep.* 9, 752–772. doi:10.1016/j.egyr.2022.12.034

Amry, Y., Elbouchikhi, E., Le Gall, F., Ghogho, M., and El Hani, S. (2023). Optimal sizing and energy management strategy for EV workplace charging station considering PV and flywheel energy storage system. *J. Energy Storage* 62, 106937. doi:10.1016/j.est.2023.106937

Ang, T.-Z., Salem, M., Kamarol, M., Das, H. S., Nazari, M. A., and Prabaharan, N. (2022). A comprehensive study of renewable energy sources: classifications, challenges and suggestions. *Energy Strategy Rev.* 43, 100939. doi:10.1016/j.esr.2022.100939

Bai, Z., Yuan, Y., Kong, D., Zhou, S., Li, Q., and Wang, S. (2023). Potential of applying the thermochemical recuperation in combined cooling, heating and power generation: off-design operation performance. *Appl. Energy* 348, 121523. doi:10.1016/j.apenergy.2023.121523

Behzadi, A., and Sadrizadeh, S. (2023). A rule-based energy management strategy for a low-temperature solar/wind-driven heating system optimized by the machine learning-assisted grey wolf approach. *ENERGY Convers. Manag.* 277, 116590. doi:10.1016/j.enconman.2022.116590

Buttler, A., and Spliethoff, H. (2018). Current status of water electrolysis for energy storage, grid balancing and sector coupling via power-to-gas and power-to-liquids: a review. *Renew. Sustain. Energy Rev.* 82, 2440–2454. doi:10.1016/j.rser.2017.09.003

Chaichan, W., Waewsak, J., Nikhom, R., Kongruang, C., Chiwamongkhonkarn, S., and Gagnon, Y. (2022). Optimization of stand-alone and grid-connected hybrid solar/wind/fuel cell power generation for green islands: application to Koh Samui, southern Thailand. *Energy Rep.* 8, 480–493. doi:10.1016/j.egyr.2022.07.024

Das, H. S., Salem, M., Zainuri, M. A. A. M., Dobi, A. M., Li, S., and Ullah, M. H. (2022). A comprehensive review on power conditioning units and control techniques in fuel cell hybrid systems. *Energy Rep.* 8, 14236–14258. doi:10.1016/j.egyr.2022.10.407

Dowling, J. A., Rinaldi, K. Z., Ruggles, T. H., Davis, S. J., Yuan, M., Tong, F., et al. (2020). Role of long-duration energy storage in variable renewable electricity systems. *Joule* 4 (9), 1907–1928. doi:10.1016/j.joule.2020.07.007

Eltayeb, W. A., Somlal, J., Kumar, S., and Rao, S. K. (2023). Design and analysis of a solar-wind hybrid renewable energy tree. *Results Eng.* 17, 100958. doi:10.1016/j.rineng.2023.100958

Erdemir, D., and Dincer, I. (2020). Assessment of renewable energy-driven and flywheel integrated fast-charging station for electric Buses: a case study. *J. Energy Storage* 30, 101576. doi:10.1016/j.est.2020.101576

Fang, R., and Liang, Y. (2019). Control strategy of electrolyzer in a wind-hydrogen system considering the constraints of switching times. *Int. J. Hydrogen Energy* 44 (46), 25104–25111. doi:10.1016/j.ijhydene.2019.03.033

Han, Y., Shi, K., Qian, Y., and Yang, S. (2023). Design and operational optimization of a methanol-integrated wind-solar power generation system. *J. Environ. Chem. Eng.* 11 (3), 109992. doi:10.1016/j.jece.2023.109992

Huang, W., Zhang, B., Ge, L., He, J., Liao, W., and Ma, P. (2023). Day-ahead optimal scheduling strategy for electrolytic water to hydrogen production in zero-carbon parks type microgrid for optimal utilization of electrolyzer. *J. Energy Storage* 68, 107653. doi:10.1016/j.est.2023.107653

Hutchinson, A. J., and Gladwin, D. T. (2023). Capacity factor enhancement for an export limited wind generation site utilising a novel Flywheel Energy Storage strategy. *J. Energy Storage* 68, 107832. doi:10.1016/j.est.2023.107832

Ibáñez-Rioja, A., Järvinen, L., Puranen, P., Kosonen, A., Ruuskanen, V., Hynynen, K., et al. (2023). Off-grid solar PV–wind power–battery–water electrolyzer plant: Simultaneous optimization of component capacities and system control. *Appl. Energy* 345, 121277. doi:10.1016/j.apenergy.2023.121277

Jia, J., Wang, Y., Li, Q., Cham, Y. T., and Han, M. (2009). Modeling and dynamic characteristic simulation of a proton exchange membrane fuel cell. *IEEE Trans. Energy Convers.* 24 (1), 283–291. doi:10.1109/tec.2008.2011837

Kakavand, A., Sayadi, S., Tsatsaronis, G., and Behbahaninia, A. (2023). Techno-economic assessment of green hydrogen and ammonia production from wind and solar energy in Iran. *Int. J. Hydrogen Energy* 48 (38), 14170–14191. doi:10.1016/j.ijhydene.2022.12.285

Li, Q., Li, R., Pu, Y., Li, S., Sun, C., and Chen, W. (2021). Coordinated control of electric-hydrogen hybrid energy storage for multi-microgrid with fuel cell/electrolyzer/PV/battery. *J. Energy Storage* 42, 103110. doi:10.1016/j.est.2021.103110

Li, Y., Li, O., Wu, F., Shi, L., Ma, S., and Zhou, B. (2022). Coordinated multi-objective capacity optimization of wind-photovoltaic-pumped storage hybrid system. *Energy Rep.* 8, 1303–1310. doi:10.1016/j.egyr.2022.08.160

Liu, L., Zhai, R., and Hu, Y. (2023a). Multi-objective optimization with advanced exergy analysis of a wind-solar-hydrogen multi-energy supply system. *Appl. Energy* 348, 121512. doi:10.1016/j.apenergy.2023.121512

Liu, L., Zhai, R., and Hu, Y. (2023b). Performance evaluation of wind-solar-hydrogen system for renewable energy generation and green hydrogen generation and storage: energy, exergy, economic, and enviroeconomic. *Energy* 276, 127386. doi:10.1016/j.energy.2023.127386

Liu, Z., Liu, B., Ding, X., and Wang, F. (2022). Research on optimization of energy storage regulation model considering wind–solar and multi-energy complementary intermittent energy interconnection. *Energy Rep.* 8, 490–501. doi:10.1016/j.egyr.2022.05.062

Lüke, L., and Zschocke, A. (2020). Alkaline water electrolysis: efficient Bridge to CO2-Emission-free economy. *Chem. Ing. Tech.* 92 (1-2), 70–73. doi:10.1002/cite.201900110

Ma, X., Zhai, Y., Zhang, T., Yao, X., and Hong, J. (2023). What changes can solar and wind power bring to the electrification of China compared with coal electricity: from a cost-oriented life cycle impact perspective. *ENERGY Convers. Manag.* 289, 117162. doi:10.1016/j.enconman.2023.117162

Meng, Z., He, Q., Shi, X., Cao, D., and Du, D. (2023). Research on energy utilization of wind-hydrogen coupled energy storage power generation system. *Sep. Purif. Technol.* 313, 123439. doi:10.1016/j.seppur.2023.123439

Nasrabadi, A. M., and Korpeh, M. (2023). Techno-economic analysis and optimization of a proposed solar-wind-driven multigeneration system; case study of Iran. *Int. J. Hydrogen Energy* 48 (36), 13343–13361. doi:10.1016/j.ijhydene.2022.12.283

Nejadian, M. M., Ahmadi, P., and Houshfar, E. (2023). Comparative optimization study of three novel integrated hydrogen production systems with SOEC, PEM, and alkaline electrolyzer. *Fuel* 336, 126835. doi:10.1016/j.fuel.2022.126835

Pan, T., Wang, Z., Tao, J., and Zhang, H. (2023). Operating strategy for grid-connected solar-wind-battery hybrid systems using improved grey wolf optimization. *Electr. Power Syst. Res.* 220, 109346. doi:10.1016/j.epsr.2023.109346

Praveenkumar, S., Agyekum, E. B., Ampah, J. D., Afrane, S., Velkin, V. I., Mehmood, U., et al. (2022). Techno-economic optimization of PV system for hydrogen production and electric vehicle charging stations under five different climatic conditions in India. *Int. J. Hydrogen Energy* 47 (38), 38087–38105. doi:10.1016/j.ijhydene.2022.09.015

Prestat, M. (2023). Corrosion of structural components of proton exchange membrane water electrolyzer anodes: a review. *J. Power Sources* 556, 232469. doi:10.1016/j.jpowsour.2022.232469

Ren, G., Wang, W., Wan, J., Hong, F., and Yang, K. (2023). A novel metric for assessing wind and solar power complementarity based on three different fluctuation states and corresponding fluctuation amplitudes. *ENERGY Convers. Manag.* 278, 116721. doi:10.1016/j.enconman.2023.116721

Ruhnau, O. (2022). How flexible electricity demand stabilizes wind and solar market values: the case of hydrogen electrolyzers. *Appl. Energy* 307, 118194. doi:10.1016/j.apenergy.2021.118194

Shen, X., Zhang, X., Li, G., Lie, T. T., and Hong, L. (2018). Experimental study on the external electrical thermal and dynamic power characteristics of alkaline water electrolyzer. *Int. J. Energy Res.* 42 (10), 3244–3257. doi:10.1002/er.4076

Su, W., Zheng, W., Li, Q., Yu, Z., Han, Y., and Bai, Z. (2023). Capacity configuration optimization for green hydrogen generation driven by solar-wind hybrid power based on comprehensive performance criteria. *Front. Energy Res.* 11, 1256463. doi:10.3389/fenrg.2023.1256463

Sultan, A. J., Ingham, D. B., Ma, L., Hughes, K. J., and Pourkashanian, M. (2023). Comparative techno-economic assessment and minimization of the levelized cost of electricity for increasing capacity wind power plants by row and angle layout optimization. *J. Clean. Prod.* 430, 139578. doi:10.1016/j.jclepro.2023.139578

Superchi, F., Papi, F., Mannelli, A., Balduzzi, F., Ferro, F. M., and Bianchini, A. (2023). Development of a reliable simulation framework for techno-economic analyses on green hydrogen production from wind farms using alkaline electrolyzers. *Renew. ENERGY* 207, 731–742. doi:10.1016/j.renene.2023.03.077

Tajouo, G. F., Kapen, P. T., and Koffi, F. L. D. (2023). Techno-economic investigation of an environmentally friendly small-scale solar tracker-based PV/wind/Battery hybrid system for off-grid rural electrification in the mount bamboutos, Cameroon. *Energy Strategy Rev.* 48, 101107. doi:10.1016/j.esr.2023.101107

Tang, O., Rehme, J., and Cerin, P. (2022). Levelized cost of hydrogen for refueling stations with solar PV and wind in Sweden: on-grid or off-grid? *Energy* 241, 122906. doi:10.1016/j.energy.2021.122906

Temiz, M., and Dincer, I. (2022). Development and assessment of an onshore wind and concentrated solar based power, heat, cooling and hydrogen energy system for remote communities. *J. Clean. Prod.* 374, 134067. doi:10.1016/j.jclepro.2022.134067

Temiz, M., and Dincer, I. (2023). A new solar and wind integrated sodium fast reactor with molten salt to generate multiple useful outputs with hydrogen. *Appl. Therm. Eng.* 232, 120960. doi:10.1016/j.applthermaleng.2023.120960

Ulleberg, Ø., Nakken, T., and Eté, A. (2010). The wind/hydrogen demonstration system at Utsira in Norway: evaluation of system performance using operational data and updated hydrogen energy system modeling tools. *Int. J. Hydrogen Energy* 35 (5), 1841–1852. doi:10.1016/j.ijhydene.2009.10.077

Wang, Q., Wang, Y., and Chen, Z. (2022). Day-ahead economic optimization scheduling model for electricity–hydrogen collaboration market. *Energy Rep.* 8, 1320–1327. doi:10.1016/j.egyr.2022.08.128

Zarate-Perez, E., Santos-Mejía, C., and Sebastián, R. (2023). Reliability of autonomous solar-wind microgrids with battery energy storage system applied in the residential sector. *Energy Rep.* 9, 172–183. doi:10.1016/j.egyr.2023.05.239

Zhang, J., Kong, X., Shen, J., and Sun, L. (2023). Day-ahead optimal scheduling of a standalone solar-wind-gas based integrated energy system with and without considering thermal inertia and user comfort. *J. Energy Storage* 57, 106187. doi:10.1016/j.est.2022.106187

Zhang, W., and Maleki, A. (2022). Modeling and optimization of a stand-alone desalination plant powered by solar/wind energies based on back-up systems using a hybrid algorithm. *Energy* 254, 124341. doi:10.1016/j.energy.2022.124341

Zhao, J., Cai, S., Luo, X., and Tu, Z. (2022). Multi-stack coupled energy management strategy of a PEMFC based-CCHP system applied to data centers. *Int. J. Hydrogen Energy* 47 (37), 16597–16609. doi:10.1016/j.ijhydene.2022.03.159

Zhou, S., Bai, Z., Li, Q., Yuan, Y., and Wang, S. (2024). Potential of applying the thermochemical recuperation in combined cooling, heating and power generation: optimized recuperation regulation with syngas storage. *Appl. Energy* 353, 122128. doi:10.1016/j.apenergy.2023.122128

Nomenclature

A	area
a	ambient
C	cost
c	unit cost
D	solar irradiance
d	output standard deviation
E	capacity scale
F	faraday constant
f	inflation rate
I	current
i	interest rate
j	current density
k	fluctuation ratio
L	lifetime
l	window scale
M	mass
N	number
n	molar amount of hydrogen
P	power
p	pressure
Q	volume
s	electrode overvoltage coefficient
T	temperature
t	time
V	voltage
v	wind speed
y	the number of years

Greek

α	diode quality factor
η	efficiency
ξ	the empirical parameters
ρ	the air density
σ	the self-discharge rate of the battery
τ	the performance coefficient of the wind turbines

Subscript

AE	alkaline electrolyzer
ad	adjusted power
bat	battery
comp	compensation
FC	fuel cell
grid	on-grid
HT	hydrogen tank
inv	investment cost
O&M	operation & maintenance
PV	photovoltaic
WT	wind turbine

Abbreviations

PEMFC	proton exchange membrane fuel cell
IRR	internal rate of return
LCOE	levelized cost of electricity
RS	residual value of fixed assets
SOC	battery state of charge
SOH	state of hydrogen tank